

Statistical thermodynamics of adhesion points in supported membranes

Oded Farago

Department of Biomedical Engineering and Ilse Katz Institute for Nanoscale Science and Technology, Ben-Gurion University of the Negev, Be'er Sheva 84105, Israel.

February 5, 2022

Abstract

Supported lipid membranes are useful and important model systems for studying cell membrane properties and membrane mediated processes. One attractive application of supported membranes is the design of phantom cells exhibiting well defined adhesive properties and receptor densities. Adhesion of membranes may be achieved by specific and non-specific interactions, and typically requires the clustering of many adhesion bonds into “adhesion domains”. One potential mediator of the early stages of the aggregation process is the Casimir-type forces between adhesion sites induced by the membrane thermal fluctuations. In this review, I will present a theoretical analysis of fluctuation induced aggregation of adhesion sites in supported membranes. I will first discuss the influence of a single attachment point on the spectrum of membrane thermal fluctuations, from which the free energy cost of the attachment point will be deduced. I will then analyze the problem of a supported membrane with two adhesion points. Using scaling arguments and Monte Carlo simulations, I will demonstrate that two adhesion points attract each other via an infinitely long range effective potential that grows logarithmically with the pair distance. Finally, I will discuss the many-body nature of the fluctuation induced interactions. I will

show that while these interactions alone are not sufficient to allow the formation of aggregation clusters, they greatly reduce the strength of the residual interactions required to facilitate cluster formation. Specifically, for adhesion molecules interacting via a short range attractive potential, the strength of the direct interactions required for aggregation is reduced by about a factor of two to below the thermal energy $k_B T$.

1 Introduction

Fatty acids and other lipids are essential to every living organism. Because of their amphiphilic nature, they spontaneously self-assemble into bilayer membranes that define the limits of cells and serve as permeability barrier to prevent proteins, ions and metabolites from leaking out of the cell and unwanted toxins leaking in [1]. In euokaryotic cells, membranes also surround the organelles allowing for organization of biological processes through compartmentalization. In addition, biological membranes host numerous proteins that are crucial for the mechanical stability of the cell, and which carry out a variety of functions such as energy and signal transduction, communication, and cellular homeostasis [2].

An important aspect of biological membranes is that they are typically not free but rather confined by other surrounding membranes, adhere to other membranes, and attach to elastic networks like the cytoskeleton and the extracellular matrix. Several model systems with reduced compositional complexity have been designed to mimic biological membranes. These biomimetic systems include phospholipid bilayers deposited onto solid substrates (solid-supported membranes) [3], or on ultra-thin polymer supports (polymer-supported membranes) [4]. Placing a membrane on a flat substrate allows for the application of several different surface sensitive techniques, including atomic force microscopy, x-ray and neutron diffraction, ellipsometry, nuclear magnetic resonance, and others [5]. With the aid of biochemical tools and generic engineering, supported membranes can be functionalized with various membrane-associated proteins [6]. Synthetic supported membranes with reconstituted proteins are increasingly used as controlled idealized models for studying key properties of cellular membranes [7]. They provide a natural environment for the immobilization of proteins under nondenaturing conditions and in well-defined orientations [8]. Another attractive application of supported membranes is the design of phantom cells exhibiting well defined adhesive properties and receptor densities [9]. Using advanced imaging techniques, detailed information can be obtained about the structure of the adhesion zone between the receptor-functionalized supported membrane and ligand-containing vesicles that can bind to the supported membrane [10,11]. These studies provide insight into the dynamics of adhesion processes and the molecular interactions involved in cell adhesion [12,13]. Understanding these interactions is crucial for the development of drug delivery systems that

depend on efficient adhesion between a liposome and the plasma membrane of the target cell.

Adhesion between two membranes or between a membrane and another surface can, in principle, be facilitated by non-specific attractive interactions (e.g., Coulomb and van der Waals interactions) [14–17]. Cell adhesion, however, is usually caused by highly specific receptor molecules located at the outside of the plasma membrane of the cell, that can bind to specific ligands on the opposite surface [18, 19]. Typically, the area density of the receptor molecules located at the outside of the plasma membrane is rather low which does not lead to efficient adhesion. However, when facing a surface with enough ligands, the receptors may cluster into highly concentrated adhesion domains to establish much stronger binding [20, 21]. Formation of adhesion clusters occurs in many biological processes [22], including the binding of white blood cells to pathogens [23], cadherin-mediated adhesion of neighboring cells [24], and focal adhesion of cells to the extracellular matrix [25]. Many biophysical aspects of specific adhesion processes, ranging from the cooperativity in adhesion cluster formation to the influence of stochastic processes such as the ligand-receptor reaction kinetics, have been and continue to be studied theoretically using various models [26–37].

Adhesion induced domain formation requires some attractive intermolecular interactions between the receptor-ligand pairs. These interactions include both *direct* and *membrane-mediated* contributions. The former are typically described by pairwise potentials which are infinitely repulsive at very small molecular separations and attractive at somewhat longer (but still finite) distances [38]. Their effect can, therefore, be studied in the framework of the thoroughly researched lattice-gas model [39]. In contrast, much less is known about the membrane-mediated mechanism, which has been proposed by Braun *et al.* to explain the formation of gap junctional plaque at cell-cell interfaces [40], and whose origin can be understood as follows: Consider two adhesion bonds between two membranes or between a membrane and a surface (Fig. 1(A)). The adhesion points restrict the thermal height fluctuations of the membrane in their vicinity. This entropy loss can be minimized if the two adhesion bonds are brought to the same place (Fig. 1(B)), in which case the membrane becomes pinned at only one place rather than two. The membrane fluctuations, thus, induce an attractive potential of mean force between the adhesion bonds. This effect is often named after Casimir who predicted the existence of an attractive

force between two conducting plates, due to quantum fluctuations of the electromagnetic field in the intervening space [41]. Later, Fisher and de Gennes generalized this concept to classical interactions induced by thermal fluctuations in soft matter systems [42]. For bilayer membranes, there is a great body of theoretical work on the Casimir effect between trans-membrane proteins (see review in [43], and refs. therein). Just like adhesion bonds, membrane inclusions represent a “constraint” on the shape of the membrane and, therefore, one should expect that they also interact with each other through Casimir-like interactions. In addition to the fluctuation-induced forces, the inclusions also experience other membrane-mediated interactions which arise from the membrane curvature elasticity and from the packing of the lipids near the inclusions’ surfaces (see review in [44], and refs. therein). These other types of membrane-mediated interactions are also expected to exist between membrane adhesion bonds.

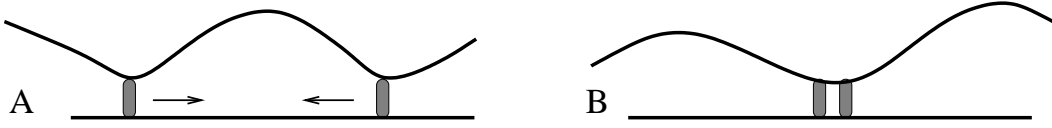


Figure 1: (A) Schematic of a membrane attached by two distant adhesion bonds to an underlying surface. There is an entropy penalty associated with each adhesion bonds due to the restrictions imposed on the membrane thermal fluctuations in their vicinity. (B) The entropy cost can be minimized by bringing the adhesion bonds close to each other, in which case the thermal fluctuations become limited at only one location. The increase in the entropy in (B) compared to (A) is the origin of the attractive fluctuation-induced interactions between the adhesion bonds.

The fundamental difficulty in attempting to provide a statistical-mechanical analysis of the aggregation behavior of the adhesion bonds is the need to integrate out the membrane degrees of freedom and write down the potential of mean force as a function of the coordinates of the adhesion sites $\phi(\vec{r}_1, \vec{r}_2, \vec{r}_3, \dots, \vec{r}_N)$. This is a non-trivial problem since the membrane-mediated potential $\phi(\vec{r}_1, \vec{r}_2, \vec{r}_3, \dots, \vec{r}_N)$ is a many-body potential which cannot be expressed as the sum of two body terms. The many-body nature of $\phi(\vec{r}_1, \vec{r}_2, \vec{r}_3, \dots, \vec{r}_N)$ is best illustrated by the following example: Consider the configuration shown in Fig. 2(A) with two adhesion bonds at located at \vec{r}_1 and \vec{r}_2 and, in comparison, the one shown in Fig. 2(B) with a single bond at \vec{r}_1 and a cluster of three bonds around \vec{r}_2 . Clearly, the spectrum of membrane thermal fluctuations in both cases is quite the same and, therefore, the adhesion bond located at \vec{r}_1 is attracted to the three-point cluster in 2(B) by the same force to which it is attracted to the single adhesion point in 2(A). If

$\phi(\vec{r}_1, \vec{r}_2, \vec{r}_3, \dots, \vec{r}_N)$ was the sum of pair interactions, the force in Fig. 2(B) would be three times larger than the force in 2(A).

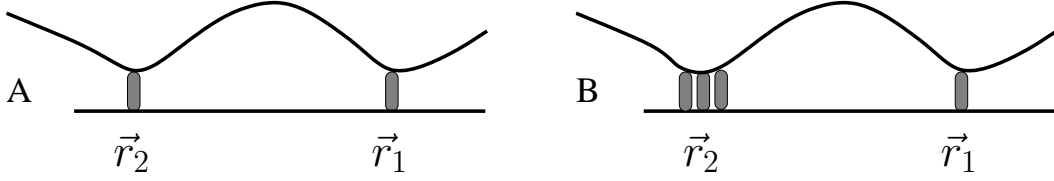


Figure 2: (A) Schematic of a supported membrane with two adhesion located at \vec{r}_1 and \vec{r}_2 . (B) Similar to (A), but with a three-bond cluster instead of a single adhesion bond in \vec{r}_2 . The adhesion bond in \vec{r}_1 is equally attracted (by a Casimir-like force) to the adhesion bond located in \vec{r}_2 in (A) and to the cluster of three adhesion bonds shown in (B).

2 Lattice-gas model for adhesion bonds in supported membranes

What is the difference between the aggregation of adhesion bonds in supported membranes and the traditional process of gas to liquid condensation? Condensation phase transitions are usually associated with a competition between the mixing entropy S which is higher in the dilute gas phase, and the interaction energy U which is lower in the condensed liquid state. The equilibrium phase corresponds to the minimum of the free energy $F = U - TS$, where T is the temperature of the system. At high T , the free energy F is “entropy-dominated” and equilibrium is attained in the gas phase. Conversely, at low T , the free energy is “energy-dominated” and, therefore, the condensed phase becomes thermodynamically more favorable. The liquid-gas phase transition can be analyzed in the framework of an Ising-like model of identical particles that populate a lattice. Excluded volume interactions between the particles are represented by the fact each lattice site can be occupied by no more than one particle. When two particles occupy nearest-neighbor sites, they interact in a pairwise fashion with an attractive energy $-\epsilon$. Denoting the occupancy of a lattice site by s_i , with $s_i = 0$ for an empty site and $s_i = 1$ for an occupied site,

the Hamiltonian of the lattice-gas model is given by

$$\mathcal{H}_{\text{LG}} = -\epsilon \sum_{i,j} s_i s_j, \quad (1)$$

where the sum runs over all the pairs of lattice nearest neighbor sites. The phase diagram of the lattice-gas model is well known. There exists a critical value α_c such that if the interaction energy $\epsilon < \alpha_c k_B T$, the particles will be distributed uniformly within the lattice. Above this critical value, $\epsilon > \alpha_c k_B T$, a uniform distribution of the particles is observed only at low concentrations of particles (“gas phase”), but upon increasing the concentration of particles, the system undergoes a first order phase transition and a second coexisting phase appears with a considerably larger concentration (“condensed phase”).

As discussed in the previous section, the aggregation process of adhesion domains involves an additional attractive potential of mean force resulting from the membrane thermal fluctuations. A lattice model where each lattice particle represents an adhesion bond in a supported membrane can, therefore, be introduced by supplementing Eq.(1) with an energy term corresponding to the fluctuation-induced interactions. Since the functional form of this many-body potential of is yet unknown, we would, at this moment, introduce it via a general potential function ϕ that depends on the coordinates of the lattice particles:

$$\mathcal{H} = -\epsilon \sum_{i,j} s_i s_j + \phi(\{s_i\}). \quad (2)$$

Our first task must be to derive an expression for $\phi(\{s_i\})$. Once this is accomplished, one can attempt to analyze the statistical mechanical properties of the model and address the question appearing at the beginning of section 2. One particular issue that we would like to address is whether the fluctuation induced attractive potential (which is of entropic origin) can win the competition against the repulsive force originating from the mixing entropy? In other words, can adhesion clusters form for purely entropic grounds, i.e. for $\epsilon = 0$ in Eq.(2)? Gas to liquid condensation transitions are generally believed to involve energy vs. entropy competition [45], but purely entropic phase transitions from a fluid (disordered) phase into a crystalline (ordered) phase are known to exist. Hard sphere systems, for instance, undergo a first order phase transition

from a low density fluid phase into a high density solid phase [46]. This transition results from the competition between two entropies - the configurational mixing entropy which is higher in the disordered phase, and the entropy associated with the free volume available for each sphere, which is higher in the ordered crystal.

3 Statistical mechanics of a membrane with one adhesion point

We start our analysis by considering the system shown schematically in Fig. 3, consisting of a membrane with bending rigidity κ that fluctuates above a flat impenetrable surface [47]. Let $h(\vec{r}) \geq 0$ be the height of the membrane with respect to the surface, and assume that the membrane is pinned to the surface at one fixed point located at \vec{r}_0 ($h(\vec{r}_0) = 0$). The elastic curvature energy of the membrane is given by the Helfrich effective Hamiltonian [48]

$$\mathcal{H}_{\text{hel}} = \int \left[\frac{\kappa}{2} (\nabla^2 h)^2 \right] \Phi(h) \delta[h(\vec{r}_0)] d^2 \vec{r}, \quad (3)$$

where Φ represents the hard wall constraint due to the surface ($\Phi = 1$ for $h \geq 0$, and $\Phi = +\infty$ for $h < 0$), δ is the Dirac delta-function, and the integration is taken over the cross sectional (projected) area of the membranes of size L^2 .

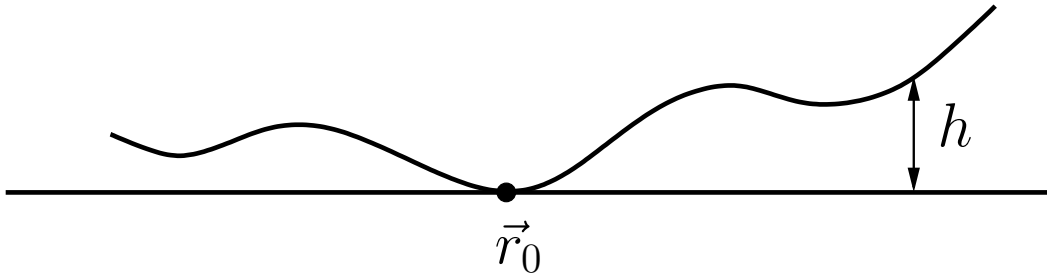


Figure 3: (A) Schematic picture of the model system consisting of a membrane that fluctuates above a flat impenetrable surface to which it is pinned at a single point.

One can calculate the partition function Z corresponding to Hamiltonian (3), by considering

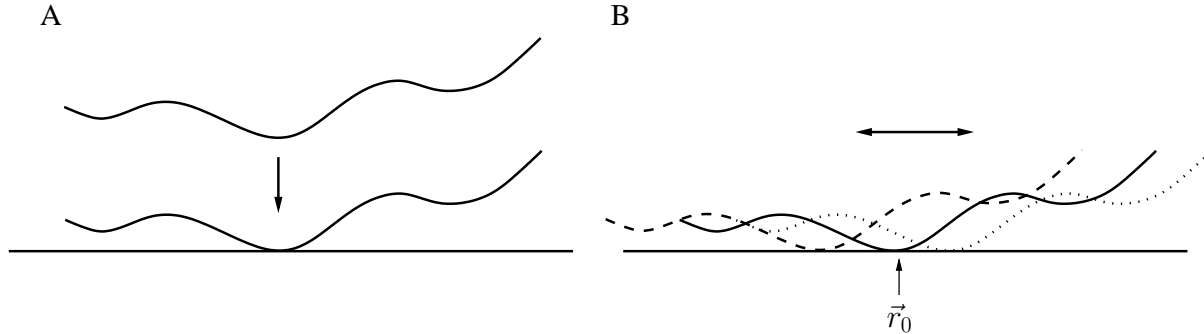


Figure 4: (A) A freely fluctuating membrane can be always translated vertically such that the point at which its height function $h(\vec{r})$ attains its global minimum is on a flat surface and the rest of the membrane is above the surface. (B) A freely fluctuating membrane can be also translated horizontally. All the membrane configurations generated in this way are similar to each other, and the one for which the point of absolute minimum is at \vec{r}_0 (represented by the solid line) is identical to the pinned membrane configuration shown in Fig. 3.

the Helfrich effective Hamiltonian of a *freely fluctuating* membrane

$$\mathcal{H}_{\text{hel}}^0 = \int \left[\frac{\kappa}{2} (\nabla^2 h)^2 \right] d^2 \vec{r}. \quad (4)$$

In this case, the associated partition function Z_{free} is readily calculated by introducing the Fourier transformation of $h(\vec{r})$: $h_q = (1/L^2) \int h(\vec{r}) \exp(i\vec{q} \cdot \vec{r})$, which decompose Hamiltonian (4) into the sum of independent harmonic oscillators

$$\mathcal{H}_{\text{hel}}^0 = \frac{l^4}{L^2} \sum_{\vec{q}} \frac{\kappa}{2} q^4 |h_q|^2, \quad (5)$$

where l is a microscopic length scale of the order of the bilayer thickness. Hamiltonian (3) which also includes the functions Φ and δ cannot be diagonalized in the same manner. However, one can relate the partition function Z of Hamiltonian (3) with the partition Z_{free} of the free membrane Hamiltonian (4), by using the following simple argument. The energy of a freely fluctuating membrane is invariant with respect to rigid-body transformations such as a vertical translation ($h(\vec{r}) \rightarrow h(\vec{r}) - h_0$) of the membrane's center of mass. Therefore, one can draw a flat surface and translate the free membrane such that the global minimum of its height function coincides with the surface (see Fig. 4(A)). The vertically translated free membrane looks very similar to the pinned membrane shown in Fig. 3(A). The only difference between

them is that the former can also glide over the surface (see Fig. 4(B)), while the latter is pinned at a fixed position on the surface. This suggests that the pinning point effectively eliminates the membrane horizontal translational degree of freedom. In a statistical mechanical language, the configurational phase space of the pinned membranes is smaller than, yet *similar* to, the phase space of a free membrane. Each subspace of identical free membrane configurations, like the ones shown in Fig. 4(B), includes one pinned membrane configuration - the configuration where the minimum of $h(\vec{r})$ is at the pinning point \vec{r}_0 (or, more precisely, within a microscopic area of size l^2 around the pinning point, where l is the spatial resolution of the continuum model). This pinned membrane configuration occupies a fraction $(l/L)^2$ of the corresponding larger free membrane configurational subspace, which implies that the partition functions of the two systems are related by $Z = (l/L)^2 Z_{\text{free}}$. The free energy is obtained from

$$F = -k_B T \ln(Z) = -k_B T \ln(Z_{\text{free}}) + 2k_B T \ln\left(\frac{L}{l}\right) \quad (6)$$

The first term on the right hand side is the free energy of the free membrane whose elastic energy is given by Helfrich Hamiltonian (3). The second term,

$$F_{\text{attachment},1} = 2k_B T \ln\left(\frac{L}{l}\right), \quad (7)$$

is the free energy cost of attaching the membrane to the surface at one point.

Following the above argument leads to a very interesting conclusion. Because of the similarity mapping that exists between the configurational phase spaces of the two problems, the statistical properties of the pinned and the free membrane must be identical to each other. This surprising result can be demonstrated by using an implicit-solvent coarse-grained (ISCG) bilayer model which enables molecular simulations of mesoscopically large bilayer membranes over relatively large time-scales [49–51]. Towards this end, we ran two independent Monte Carlo (MC) simulations - one of a free membrane (without a surface) and one of a membrane supported by a flat impenetrable surface. A snapshot from the supported membrane simulations is shown in Fig. 5. Each lipid molecule is represented in the model by a short string of three spherical beads, where one of the beads (depicted as a dark gray sphere in Fig. 5) represents the hydrophilic head group

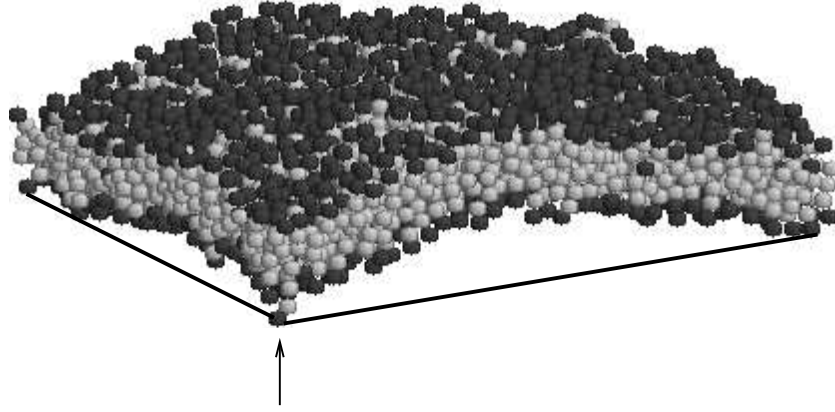


Figure 5: Equilibrium configuration of a membrane consisting of 2000 lipids. Each lipid is represented by a trimer of one “hydrophilic” bead (dark gray sphere) and two “hydrophobic” beads (light gray spheres). The membrane is fluctuating above a plane surface (frame indicated by a thick black line), while one of the hydrophilic beads (the black sphere appearing at the front of the figure and indicated by an arrow) is held on the surface at a fixed position.

and two beads (light gray spheres in Fig. 5) represent the hydrophobic tail of the lipid. In the supported membrane simulations, the head bead of one of the lipids (appearing in the corner at the front of the figure and indicated by an arrow) was fixed to a flat surface which the lipids were not allowed to cross. We measured the Fourier spectrum of the membrane height function. For the free membrane, the application of the equipartition theorem to the Fourier-space representation of the Helfrich Hamiltonian (5) yields the following relationship between the mean squared amplitude of the Fourier modes (“spectral intensity”) and the wave-vector q :

$$\langle |h_q|^2 \rangle = \frac{k_B T L^2}{\kappa l^4 q^4}. \quad (8)$$

Fig. 6 depicts the results of our MC simulations for the spectral intensity vs. the wavenumber $n = qL/(2\pi)$. The figure show that, in agreement with our predictions: (i) the free (open circles) and pinned (solid circles) membranes exhibit the same statistics of thermal height fluctuations, and (ii) the spectral intensities of both membranes follow the n^{-4} power-law dependence anticipated by Eq.(8) (dashed line).

One can reverse the argument and derive Eq.(7) starting from the assumption that the spectral intensity of the supported membrane is identical to that of a free membrane and, therefore, can be described by Eq.(8). The derivation proceeds as follows: First, from Eq.(8), one can

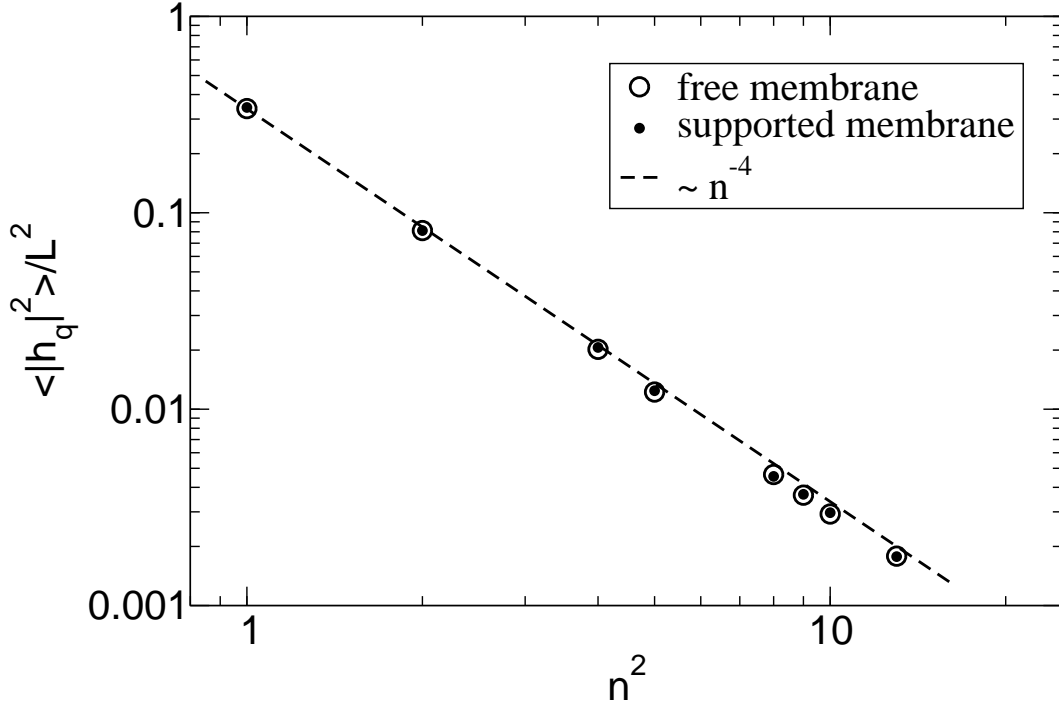


Figure 6: The mean square amplitude of the thermal height fluctuations as a function of the wavenumber n . The results from the supported membrane simulations are shown by small solid circles. These results are essentially identical to those obtained from simulations of a free membrane which are represented by larger open circles. The dashed line indicates the asymptotic $\langle |h_q|^2 \rangle \sim n^{-4}$ power law for small n . (adapted from [47])

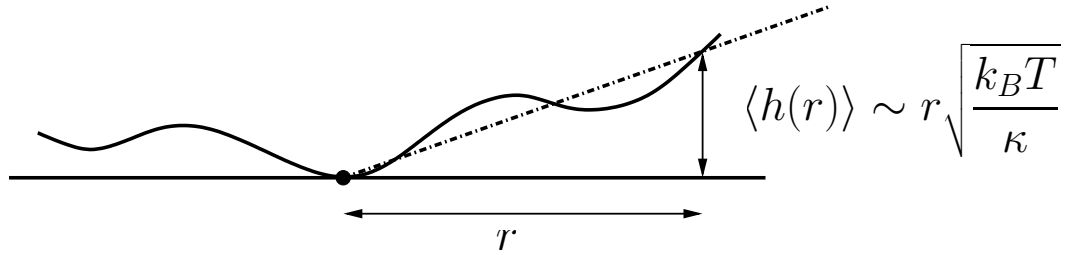


Figure 7: The fact that the statistics of thermal height fluctuations is not affected by the single pinning point implies that the typical height of the fluctuations scales linearly with the distance from the pinning site.

straightforwardly show that the typical height at which the membrane undulates above the surface at a distance r away from the pinning point scales linearly with r [47, 52] (see Fig. 7):

$$u(r) \equiv \langle h(r) \rangle \sim r \sqrt{\frac{k_B T}{\kappa}}. \quad (9)$$

There is a repulsive force acting between the fluctuating membrane and the underlying surface, caused by their mutual steric hindrance. Helfrich [53] showed that the associated repulsive interaction free energy density (per unit area) has the following scaling behavior $V(r) \sim (k_B T)^2 / \kappa u(r)^2$ which, together with Eq.(9), yields

$$V(r) \sim \frac{k_B T}{r^2}. \quad (10)$$

By integrating this energy density over the projected area of the membrane, one derives Eq.(7) up to a numerical prefactor

$$F_{\text{attachment},1} = \int V(r) d^2 \vec{r} \sim \int_l^L 2\pi r \frac{k_B T}{r^2} dr = C k_B T \ln \left(\frac{L}{l} \right). \quad (11)$$

To set $C = 2$, as in Eq.(7), one needs to replace the scaling relation Eq.(10) with the equality

$$V(r) = \frac{1}{\pi} \frac{k_B T}{r^2}. \quad (12)$$

4 Fluctuation induced attraction between two adhesion points

As noted by Helfrich [53], the free energy density Eq.(12) due to the steric hindrance between the two surfaces (i.e., the fluctuating membrane and the underlying supporting surface) is directly related to the rate of collisions between them. In other words, the probability density that the membrane hits the supporting surface at a distance r from the pinning point exhibit the same dependence on r as $V(r)$:

$$p[h(\vec{r}) = 0] \sim \frac{1}{r^2}. \quad (13)$$

This relationship provides the information needed for calculating the fluctuation induced attractive potential between two adhesion points. This is done by regarding the point of collision between the membrane and the surface as a second pinning point which can diffuse across the surface. In this context, the probability density $p[h(\vec{r}) = 0]$ is identified with the pair correlation

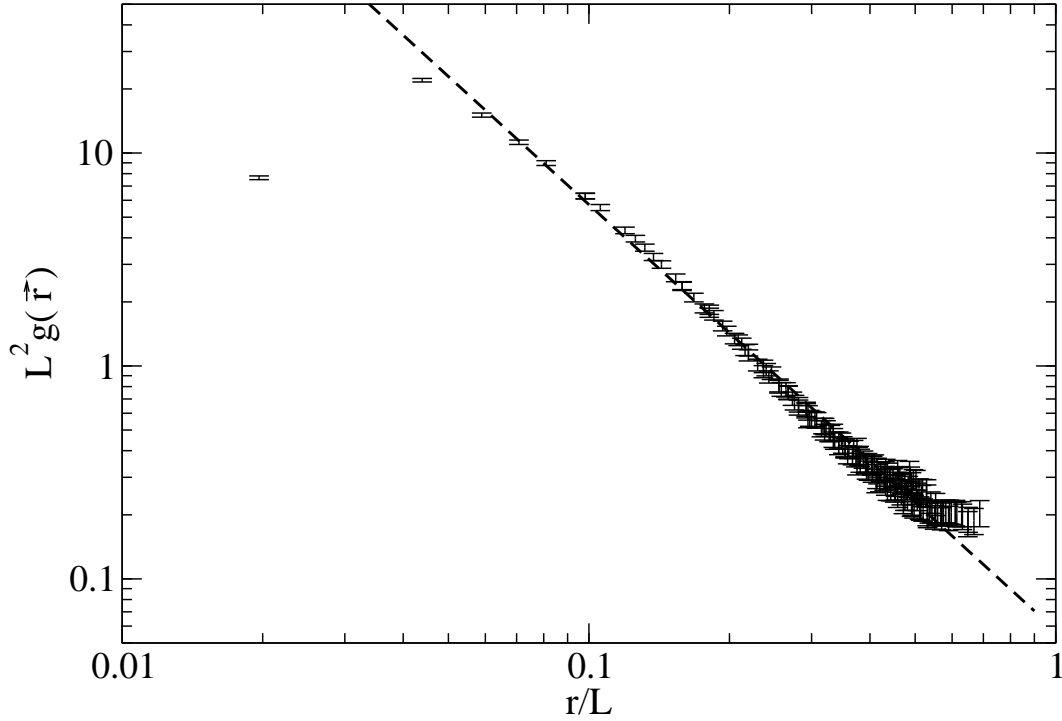


Figure 8: The pair correlation function, $g(\vec{r})$, of a non-stressed membrane vs. the pair distance r . The slope of the dashed straight line is -2 . (adapted from [54])

function between the adhesion points which, therefore, also follows the scaling form

$$g(\vec{r}) \sim \frac{1}{r^2}. \quad (14)$$

By definition, the pair potential of mean force is given by

$$\phi(\vec{r}) \equiv -k_B T \ln[g(\vec{r})] = 2k_B T \ln(r), \quad (15)$$

which is an infinitely long range attractive potential that does not depend of the bending rigidity of the membrane, κ .

The validity of Eq.(14) can be tested by using MC simulations of the ISCG model shown in Fig. 5 with two lipid heads attached to surface - one fixed at the origin and the other allowed to diffuse on the flat surface. The pair correlation function is then directly computed by sampling the position of the mobile adhesion point. Our results [54], which are shown in Fig. 8, agree very well with Eq.(14). The slope of the straight line on the log-log plot is equal to -2 . The

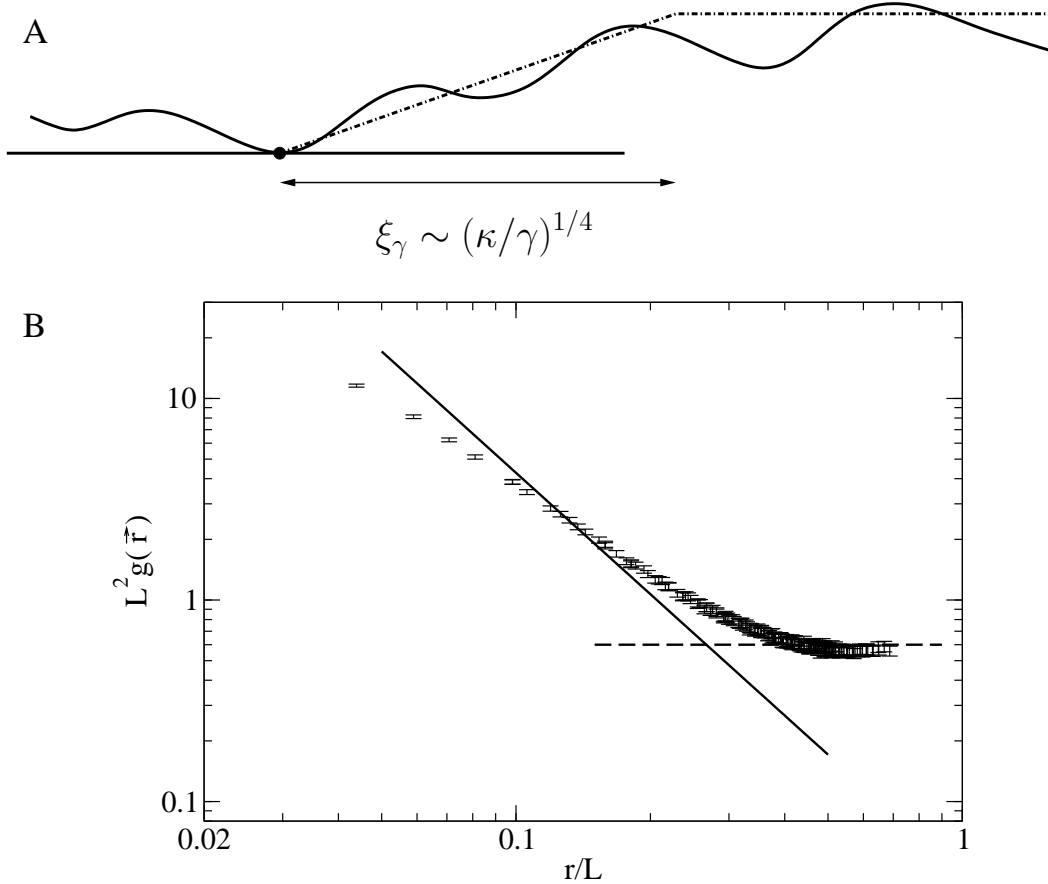


Figure 9: (A) The typical height of the fluctuations of a supported membrane experiencing a harmonic confining surface potential, grows linearly close to the pinning point and saturates at large distances. (B) The pair correlation function, $g(\vec{r})$, of a such a membrane vs. the pair distance r . The slopes of the solid and dashed straight lines are -2 and 0 , respectively. ((B) is adapted from [54])

deviations from the power law behavior $g(\vec{r}) \sim 1/r^2$ at small values of r ($r/L < 0.05$) are related to the breakdown of the continuum description of the Helfrich Hamiltonian at small spatial scales. At small separations, the molecular nature of the lipids becomes important and the radial pair distribution function is dominated by the depletion shells around the lipids.

What if, in addition to the excluded volume repulsion, the membrane and the surface also interact via an attractive potential of somewhat longer range? Let us consider, for instance, the case when a harmonic confining potential is added to the Helfrich Hamiltonian:

$$\mathcal{H} = \int \left[\frac{\kappa}{2} (\nabla^2 h)^2 + \frac{\gamma}{2} h^2 \right] d^2 \vec{r}. \quad (16)$$

For the harmonically confined membrane, one can define the length scale $\xi_\gamma \sim (\kappa/\gamma)^{1/4}$ which marks the transition between two scaling regimes. For $r \ll \xi_\gamma$, the thermal fluctuations are governed by the bending rigidity term in Hamiltonian (16), while for $r \gg \xi_\gamma$ the harmonic confinement term becomes dominant. The latter term is a local one, which implies that the influence of the adhesion point becomes screened at large distances. In the case of a single adhesion point, the height of the fluctuations is now given by (compare with Eq.(9))

$$\langle h(r) \rangle \sim \begin{cases} r \sqrt{\frac{k_B T}{\kappa}} & \text{for } r \ll \xi_\gamma \\ \xi_\gamma \sqrt{\frac{k_B T}{\kappa}} & \text{for } r \gg \xi_\gamma \end{cases}, \quad (17)$$

as illustrated schematically in Fig. 9(A). The correlation function of a pair of adhesion points is given by (compare with Eq.(14))

$$g(\vec{r}) \sim \begin{cases} r^{-2} & \text{for } r \ll \xi_\gamma \\ r^0 & \text{for } r \gg \xi_\gamma \end{cases}. \quad (18)$$

The results of MC simulations of an ISCG molecular model of a harmonically confined membrane verify this crossover between the two scaling regimes of $g(\vec{r})$ (see Fig. 9(B)).

The energy of a membrane subjected to lateral surface tension $\sigma > 0$ is given by the following Hamiltonian

$$\mathcal{H} = \int \left[\frac{\kappa}{2} (\nabla^2 h)^2 + \frac{\sigma}{2} (\vec{\nabla} h)^2 \right] d^2 \vec{r}. \quad (19)$$

Scaling arguments [54] show that, in this case, the pair correlation function exhibits behavior intermediate between Eqs.(14) and (18):

$$g(\vec{r}) \sim \begin{cases} r^{-2} & \text{for } r \ll \xi_\sigma \\ r^{-1} & \text{for } r \gg \xi_\sigma \end{cases}, \quad (20)$$

where the crossover length $\xi_\sigma \sim (\kappa/\sigma)^{1/2}$. This scaling form is also confirmed by MC simulations (see Fig. 10).

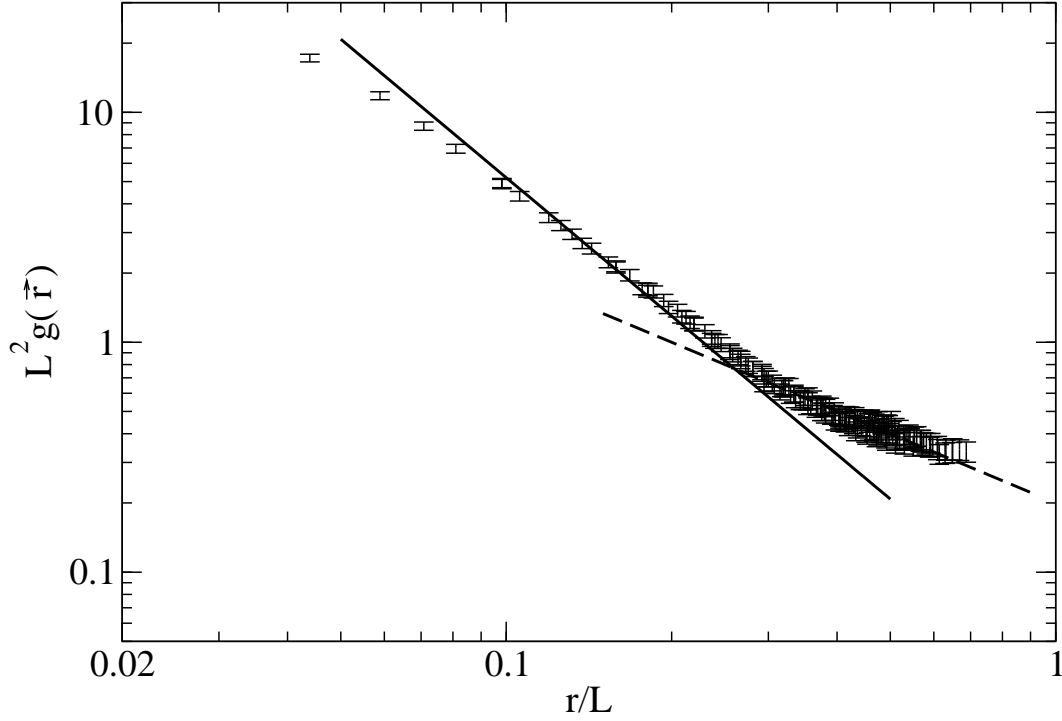


Figure 10: The pair correlation function, $g(\vec{r})$, of a supported membrane under tension vs. the pair distance r . The slopes of the solid and dashed straight lines are -2 and -1 , respectively. (adapted from [54])

5 The strength of the fluctuation-induced attraction

One of the main questions we aim to explore is whether the fluctuation-induced interactions are sufficiently strong to allow the formation of adhesion clusters. In the case of two adhesion points the answer is no. Despite of the attractive force between the adhesion points, they remains unbound and their mean pair separation grows linearly with the system size L . More generally, if the pair correlation function decays algebraically at large distance, $g(\vec{r}) \sim r^{-c}$, the mean pair separation is given by

$$\langle r \rangle \sim \frac{\int_l^L r^2 g(\vec{r}) dr}{\int_l^L r g(\vec{r}) dr} \sim \begin{cases} L & \text{for } c < 2 \\ L / \ln L & \text{for } c = 2 \\ L^{3-c} & \text{for } 2 < c < 3 \\ \ln L & \text{for } c = 3 \\ l & \text{for } c > 3 \end{cases} . \quad (21)$$

The physically relevant cases in Eq.(21) are $c = 2, 1$, and 0 which, respectively, correspond to pinned, pinned-stressed, and pinned-confined membranes. In all of these cases, $\langle r \rangle$ grows with the size of the system.

Another quantity of interest is the mean number $\langle C \rangle$ of contacts between the surface and a membrane with one adhesion point. As discussed in section 4, the probability density that membrane comes into contact with the surface at a distance r from the pinning point has the same scaling form as the pair correlation function $g(\vec{r})$. Thus,

$$\langle C \rangle \sim \int_l^L g(\vec{r}) r dr \sim \begin{cases} (L/\xi_\gamma)^2 & \text{for } c = 0 \\ L/\xi_\sigma & \text{for } c = 1 \\ \ln(L/l) & \text{for } c = 2 \end{cases} . \quad (22)$$

We can use this last result to generalize and recalculate the attachment free energy of one adhesion point, Eq.(7). Our original derivation of Eq.(7) was based on the argument that the configuration phase space of a pinned membrane comprises a small subspace within the configuration phase space of a free membrane. More precisely, we argued that this subspace includes the free membrane configurations in which the global minimum of the height function occurs at the pinning point of the corresponding supported membrane. We further argued that the relative size of the subspace is $(l/L)^2$, which was based on the assumption that typically there is only one contact point with the surface and, therefore, this contact point must be the adhesion site. However, as we see from Eq.(22), a typical configuration makes $\langle C \rangle$ contacts with the surface. Therefore, the partition functions of the two problems (free vs. pinned membranes) are actually related by $Z = [\langle C \rangle (l/L)^2] Z_{\text{free}}$. The attachment free energy is given by

$$F_{\text{attachment},1} = -k_B T \ln \left(\frac{\langle C \rangle l^2}{L^2} \right) = \begin{cases} 2k_B T \ln(\xi_\gamma/l) & \text{for } c = 0 \\ k_B T \ln(L/l) + k_B T \ln(\xi_\sigma/l) & \text{for } c = 1 \\ 2k_B T \ln(L/l) - k_B T \ln[\ln(L/l)] & \text{for } c = 2 \end{cases} . \quad (23)$$

Notice that for sufficiently large L , $F_{\text{attachment},1}(c = 2) > F_{\text{attachment},1}(c = 1) > F_{\text{attachment},1}(c = 0)$. Indeed, the attachment of a free membrane to a surface is likely to be more costly than the attachment of stressed and harmonically confined membranes that exhibit reduced fluctuations

and, thus, remain close to the surface anyway.

6 The many-body problem

Let us look back at Fig. 8 which shows the pair correlation function between two adhesion points. The figure demonstrates that the scaling form Eq.(14) holds over almost the entire range of pair separations considered ($l < r < L/\sqrt{2}$). The deviations from the power law at small pair distances arising from the short range depletion forces between lipids have already been discussed in section 4. What is quite surprising, though, is the pretty good agreement between the MC results and Eq.(14) at large pair distances. Eq.(14) has been derived for two adhesion points in a very large membrane, neglecting boundary effects. In the simulations the conditions are different - the membrane has a finite size and periodic boundary conditions are employed to reduce the finite size effects. Thus, each adhesion point interacts not only with the other adhesion point but also with its infinite array of periodic images. Nevertheless, the existence of periodic images seems to have a very small impact on the results. This observation is particularly unexpected for $r > L/2$ corresponding to situations where one of the adhesion points is equally close to two images of the other adhesion point. The only possible way to explain this surprising observation is to assume that the periodic images of the adhesion points are largely screened. This assumption is consistent with the following physical picture: The membrane mediated interactions originate from the entropic cost due to the suppression of the membrane thermal undulations. Thus, the presence of each adhesion point is felt only in the region where it affects the fluctuations and cause their reduction, while outside of this region, the adhesion point is effectively screened. In this perspective, the idea that distant adhesion points are screened seems logical. The fluctuations vanish at each adhesion point, irrespective of the distribution of the others. Moreover, in the immediate vicinity of each adhesion point, one expects the amplitude of the fluctuations to depend only on the distance from that adhesion point. If the membrane is neither stressed nor experiencing a confining surface potential, the amplitude of the fluctuations in this region grows linearly with the distance r from the adhesion point, as given by Eq.(9). We now wish to introduce a more general expression that holds over the entire area of the membrane and coincides with Eq.(9) close to every adhesion point. Our suggestion is as follows [55]: In

each unit area of the membrane, the mean height of the membrane above the surface is given by (compare with Eq.(9))

$$\langle h(r) \rangle \sim d_{\min} \sqrt{\frac{k_B T}{\kappa}}, \quad (24)$$

where d_{\min} is the distance of the unit area from the *nearest* adhesion point. We also replace r with d_{\min} in Eq.(12) for the attachment free energy density, which now reads

$$V(r) = \frac{1}{\pi} \frac{k_B T}{d_{\min}^2}. \quad (25)$$

The total attachment free energy of a given distribution of adhesion points is obtained by integrating the attachment free energy density Eq.(25) over the entire membrane area. This calculation is done by constructing the Voronoi diagram of the distribution of adhesion points, integrating the free energy density with each cell (where in each cell the distance is measured from the adhesion point located in the cell, and a small region of microscopic size l around the point is excluded from the integral), and summing the contributions of the different cells:

$$F_{\text{attachment}} = \sum_{i=1}^{N_{\text{cell}}} \int \frac{k_B T}{\pi r^2} d^2 \vec{r} \quad (26)$$

In a lattice-gas model, the discrete analog of this expression applies

$$F_{\text{attachment}} = \sum_i \frac{k_B T}{\pi} \left(\frac{l}{d_{\min}} \right)^2 (1 - s_i), \quad (27)$$

where the sum run over all the empty lattice sites ($s_i = 0$) and l^2 is the area per lattice site.

As discussed in section 2, our main goal is to develop and use a lattice-gas model for the aggregation problem of adhesion points. In the model, each lattice point represents an adhesion point between the membrane and surface. The energy of a given configuration of lattice points is given by Eq.(2), where the first term represents the short-range attraction between adhesion points and the second term is a many-body fluctuation-induced potential $\phi(\{s_i\})$. Our journey to derive an expression for $\phi(\{s_i\})$ started in section 3, and has finally reached the end. $\phi(\{s_i\})$ is a potential of mean force which, for a given distribution of adhesion points, is determined by

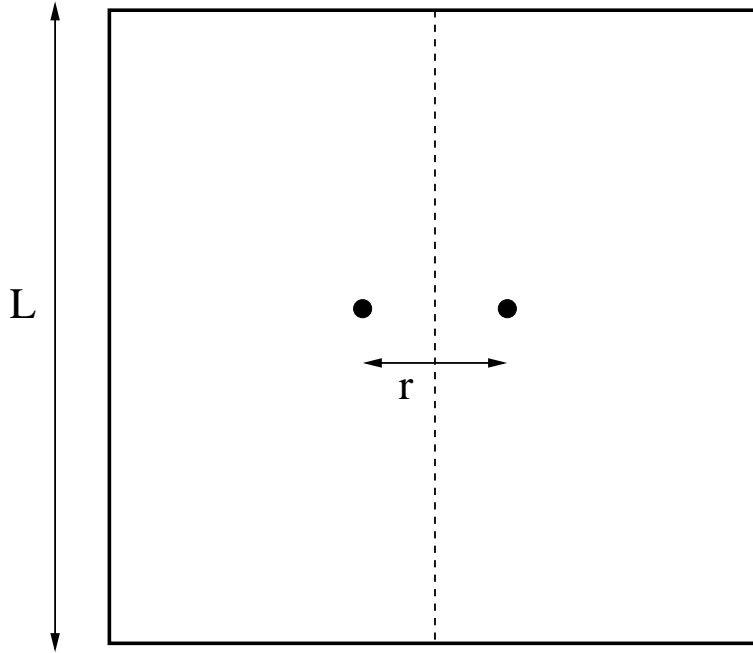


Figure 11: Schematic of a square membrane of linear size L with two adhesion points located at $(x, y) = (\pm r/2, 0)$. The dashed line shows the boarder between the Voronoi cells of the adhesion points.

tracing over all the relevant membrane configurations and calculating the free energy penalty associated with the reduced thermal fluctuations. Eq.(27) provides this expression by assigning a free energy cost with each empty lattice site that represents a fluctuating unit area of the supported membrane. Introducing Eq.(27) into Eq.(2), yields the energy function of our lattice-model of adhesion points

$$\mathcal{H} = -\epsilon \sum_{i,j} s_i s_j + \sum_i \frac{k_B T}{\pi} \left(\frac{l}{d_{\min}} \right)^2 (1 - s_i). \quad (28)$$

6.1 The two-body problem revisited

Let us see how one can re-derive Eq.(15) for the pair potential of mean force by calculating the attachment free energy Eq.(26). Towards this end, consider the membrane shown schematically in Fig. 11 with two adhesion points, each of which located a distance $r/2$ from the center of the membrane. The dashed line shows the boarder between the Voronoi cells of the adhesion points, where each cell extends over half of the area of the membrane. For the configuration shown in

Fig. 11, the attachment free energy Eq.(26) reads:

$$\begin{aligned}
F_{\text{attachment},2} &= 4 \int_0^{L/2} dy \left[\int_0^{(r-l)/2} dx \frac{k_B T}{\pi [y^2 + (x - r/2)^2]} \right. \\
&\quad \left. + \int_{(r+l)/2}^{L/2} dx \frac{k_B T}{\pi [y^2 + (x - r/2)^2]} \right]. \tag{29}
\end{aligned}$$

Integrating over y yields,

$$\begin{aligned}
F_{\text{attachment},2} &= \frac{4k_B T}{\pi} \left[\int_0^{(r-l)/2} \frac{dx}{|x - r/2|} \tan^{-1} \left(\frac{L}{2|x - r/2|} \right) \right. \\
&\quad \left. + \int_{(r+l)/2}^{L/2} \frac{dx}{|x - r/2|} \tan^{-1} \left(\frac{L}{2|x - r/2|} \right) \right]. \tag{30}
\end{aligned}$$

Assuming that $l < r \ll L$, the inverse tangent function in Eq.(30) can be approximated by the constant value of $\pi/2$ over most of the integration range. With this approximation, one gets

$$F_{\text{attachment},2}(r, L) \simeq 2k_B T \ln \left(\frac{L}{l} \right) + 2k_B T \ln \left(\frac{r}{l} \right) = F_{\text{attachment},1}(L) + \phi(r). \tag{31}$$

The first term in eq.(31) is the free energy cost of a single adhesion site [Eq.(7)], which is the expected value when the two adhesion points coincide ($r \simeq l$) to form a single cluster. The second term, which represents the additional free energy cost associated with the separation of the adhesion points, is identified as the fluctuation induced pair potential, in agreement with Eq.(15).

6.2 Mean field theory

We now come back to the many-body problem and start with a mean field analysis of our lattice model Hamiltonian (28). Let us consider a lattice of N_s sites of which $N \leq N_s$ sites are occupied by adhesion points. Let us further assume that the adhesion points form $N_c \leq N$ adhesion clusters. The free energy of system includes three contributions: (i) the mixing entropy of the adhesion clusters, F_{mix} , (ii) the lattice-gas energy, E_{LG} , of the direct interactions between the adhesion points [first term in Eq.(28)], and (iii) the attachment free energy, F_N [second term in

Eq.(28)]. The first free energy contribution is given by

$$\frac{F_{\text{mix}}}{k_B T} = N_c \left[\ln \left(\frac{N_c}{N_s} \right) - 1 \right] + \frac{1}{2} c \left(\frac{N_c^2}{N_s} \right), \quad (32)$$

where c is the second virial coefficient. On average, each cluster consists of (N/N_c) adhesion points; and if we assume that it has a roughly circular shape than $c \simeq 4(N/N_c)$. Denoting the number densities of the adhesion points by $\rho = N/N_s$, and of the clusters by $\rho^* = N_c/N_s \leq \rho$, the free energy of mixing per lattice site is given by

$$\frac{F_{\text{mix}}}{N_s k_B T} = \rho^* [\ln(\rho^*) - 1] + 2\rho\rho^*. \quad (33)$$

The second contribution to the free energy is due to the direct interactions between the adhesion points. The ground state of the interaction energy E_{LG} is achieved when a single circular adhesion domain with minimal surface is formed. If we set the ground state as the reference energy, the energy of an ensemble of clusters can be estimated as being proportional to the total length of the domain boundaries. For N_c circular clusters of size (N/N_c) we have

$$\frac{E_{\text{LG}}}{N_s k_B T} = \lambda \frac{N_c}{N_s} \sqrt{\frac{N}{N_c}} = \lambda \sqrt{\rho\rho^*}, \quad (34)$$

where λ , the associated dimensionless line tension, is proportional to the interaction energy ϵ

$$\lambda = 2\sqrt{\pi} B \epsilon, \quad (35)$$

and B is the mean number of nearest-neighbor vacant sites per occupied site on the boundary of a cluster ($B \rightarrow 1$ for very large clusters). The sum of free energy contributions (33) and (34) constitutes the total free energy density (per lattice site) of a 2D lattice gas of clusters:

$$\frac{F_{\text{LG}}}{N_s k_B T} = \rho^* \ln(\rho^*) - \rho^* + 2\rho\rho^* + \lambda \sqrt{\rho\rho^*}. \quad (36)$$

The third contribution to the attachment free energy can be estimated as follows. The clusters form N_c Voronoi cells, each of which has on average an area of $A_{\text{vor}} = (N_s/N_c)l^2$. The attachment

free energy of each Voronoi cell is given by an equation similar to Eq.(7) for the attachment free energy of one adhesion point, but with A_{vor} instead of the total membrane area L^2 . Thus

$$F_N = N_c \left[k_B T \ln \left(\frac{N_s}{N_c} \right) \right], \quad (37)$$

and the attachment free energy density is given by

$$\frac{F_N}{N_s k_B T} = -\rho^* \ln(\rho^*), \quad (38)$$

which eliminates the first term in the lattice-gas free energy density [Eq.(36)], yielding

$$\frac{F}{N_s k_B T} = \frac{F_{\text{LG}}}{N_s k_B T} + \frac{F_N}{N_s k_B T} = -\rho^* + 2\rho\rho^* + \lambda\sqrt{\rho\rho^*}. \quad (39)$$

We consider a low density of adhesion sites $\rho \ll 1$, which also implies a low number density of adhesion clusters since $\rho^* \leq \rho$. By minimizing the free energy density we obtain the equilibrium value of the ρ^* for the standard lattice-gas model [Eq.(36)] and for the adhesion points of a fluctuating supported membrane [Eq.(39)]. In both cases, the system undergoes a first order phase transition at $\lambda_1(\rho)$ from the gas phase ($\rho^* = \rho$) to a condensed phase consisting of only a few clusters ($\rho^* \sim 0$). Also, in both cases, the free energy reaches a maximum at intermediate densities ($0 < \rho^* < \rho$). This free energy barrier for condensation disappears at the spinodal point $\lambda_2(\rho) > \lambda_1(\rho)$. For the lattice-gas problem we find

$$\begin{aligned} \lambda_1^{\text{LG}} &= 1 - 2\rho - \ln(\rho) \\ \lambda_2^{\text{LG}} &= -4\rho - 2\ln(\rho), \end{aligned} \quad (40)$$

while for the adhesion points of fluctuating membranes we have

$$\begin{aligned} \lambda_1 &= 1 - 2\rho \\ \lambda_2 &= 2 - 4\rho = 2\lambda_1. \end{aligned} \quad (41)$$

The results of Eqs.(40) and (41) are summarized in Fig. 12(A) and 12(B), respectively. The

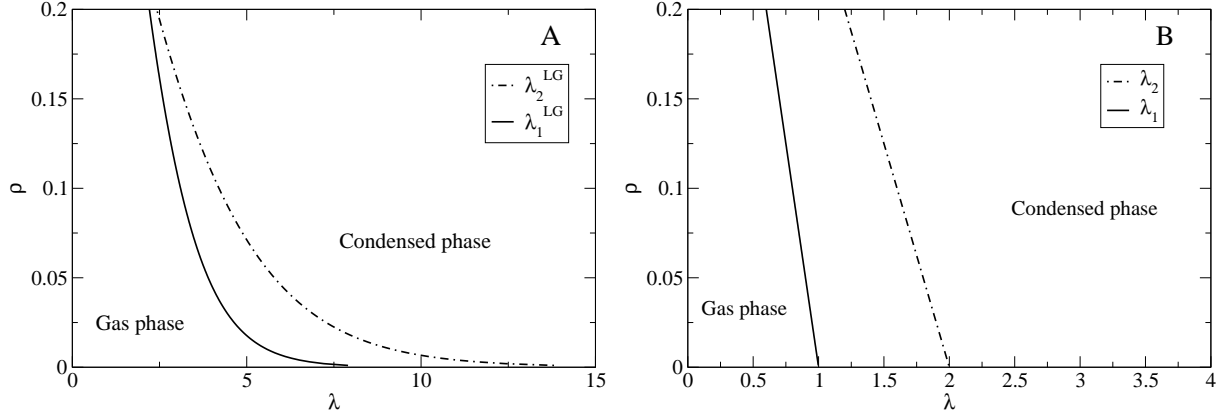


Figure 12: The phase diagram of the adhesion sites calculated within the mean field approximation. (A) Eq.(40) for the standard 2D lattice-gas model. (B) Eq.(41) for adhesion points of fluctuating membranes. λ_1 and λ_2 represent the first-order transition and spinodal lines, respectively. (adopted from [55])

important points in the results are that: (i) $\lambda_1 > 0$, which means that the fluctuation induced interactions alone are *not* sufficient to induce aggregation of adhesion domains, but (ii) they greatly reduce the strength of the direct interactions required to facilitate cluster formation since $\lambda_1 < \lambda_1^{\text{LG}}$ (and also $\lambda_2 < \lambda_2^{\text{LG}}$). Below, we support these conclusions with MC simulations and show that for adhesion points of fluctuating membranes, the site-site cohesive energy ϵ for the onset of aggregation falls below the thermal energy $k_B T$.

6.3 Monte Carlo simulation

To further investigate the aggregation behavior in supported membranes, we performed MC simulations of both our lattice model of adhesion points and of the standard 2D lattice-gas model [55]. We simulated the system at two different densities $\rho = N/N_s = 0.05$ and $\rho = 0.1$, and for various values of ϵ ranging from 0 to $3 k_B T$. Snapshots taken from simulations for $\epsilon = 1 k_B T$ and $\rho = 0.1$ are shown in Fig. 13. Fig. 13(A) shows the initial configuration where the points are randomly distributed on the lattice. Figs. 13(B) and 13(C) show, respectively, typical equilibrium configurations of the standard lattice-gas model and of our model of adhesion points. One clearly sees that for the same strength of the interaction energy $\epsilon = 1 k_B T$, the standard lattice gas model remains in the gas phase, while the adhesion points (that, in addition to the direct interactions, also attract each other via the fluctuation-induced mechanism) condense into

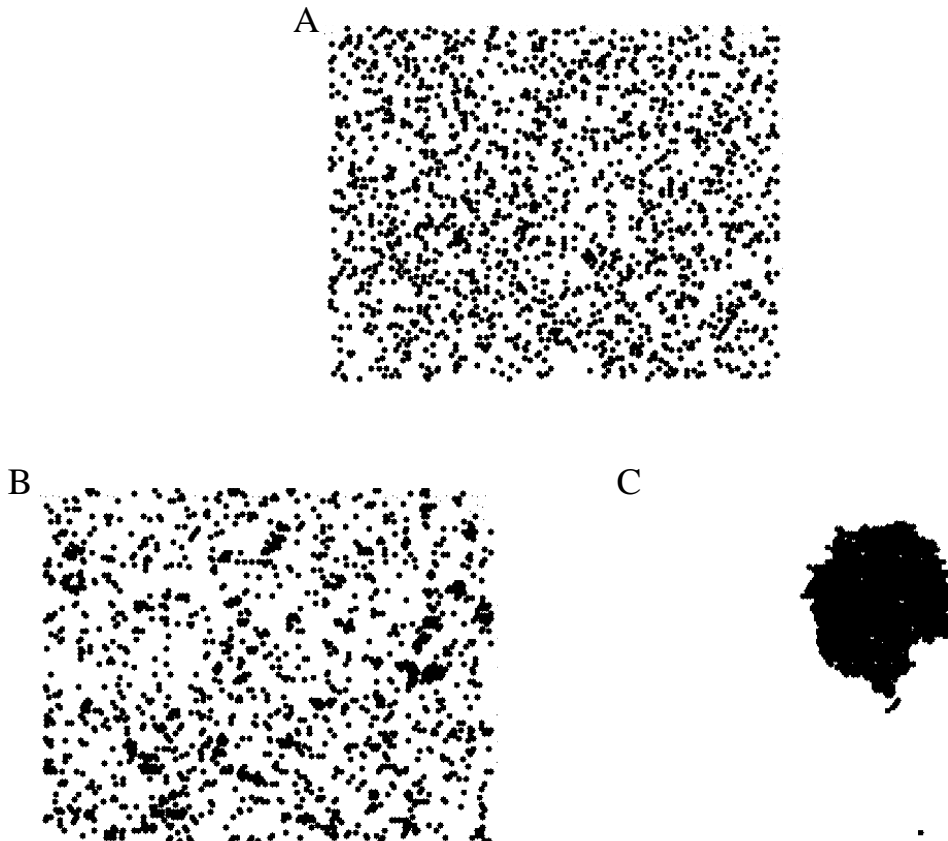


Figure 13: (A) Initial configurations of the simulations in which the points are randomly distributed on the lattice. (B) Representative equilibrium configurations of the standard lattice gas model for $\rho = 0.1$ and $\epsilon = 1k_B T$. (C) Representative equilibrium configurations of our lattice model of adhesion points for the same values of ρ and ϵ as in (B).

a large cluster containing almost all the adhesion points.

In order to determine the onset of the gas to liquid transition, we measured the average number of clusters in the system (where a cluster is defined as a set of neighboring occupied sites), and the mean value of the energy of direct interactions between sites, $\langle E_{LG} \rangle$ [first term in Eq.(28)]. Our results are summarized in Fig. 14(A) (for $\rho = 0.05$) and 14(B) (for $\rho = 0.1$). For each ρ , we measured these quantities both for the standard lattice-gas model (open symbols and dash-dotted lines in Fig. 14) and for the adhesion points model (solid symbols and solid lines in Fig. 14). The number of clusters is denoted by squares (values on the right y -axis of the figures), while $\langle E_{LG} \rangle$ is represented by circles (values on the left y -axis). The gas phase is characterized by a large number of small clusters, some of which may be of the size of a single

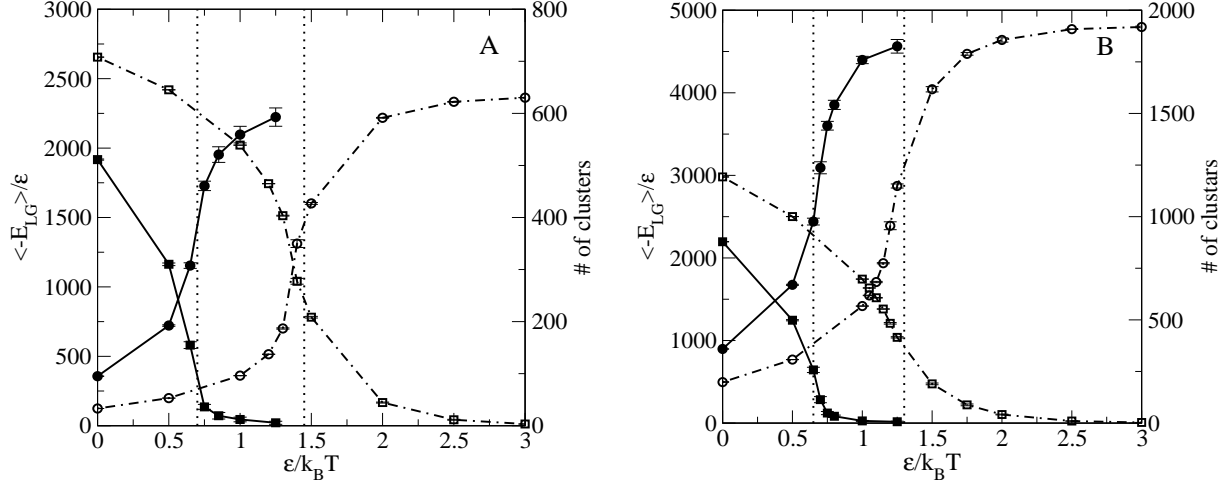


Figure 14: Left y -axis: The energy of direct interactions between sites, $\langle E_{LG} \rangle$, as a function of ϵ , for $\phi = 0.05$ (A) and $\phi = 0.1$ (B). Solid circles - results for our model for adhesion points. Open circles - results for the standard lattice-gas model. Right y -axis: The number of clusters as a function of ϵ , for $\phi = 0.05$ (A) and $\phi = 0.1$ (B). Solid squares - results for our model for adhesion points. Open squares - results for the standard lattice-gas model. (adapted from [55])

site. Furthermore, since each occupied site has a relatively small number of neighboring occupied sites, the mean configurational energy $\langle -E_{LG} \rangle$ is relatively low. Conversely, when the sites form large clusters in the condensed phase, $\langle -E_{LG} \rangle$ is high, and the total number of clusters decreases (and in many cases, especially for large values of ϵ , we simply observe only a single cluster in our system). Fig. 14 exhibits an abrupt, clearly first-order, transition from a gas phase with a large number of clusters and small $\langle -E_{LG} \rangle$ to a condensed state with a small number of clusters and large $\langle -E_{LG} \rangle$. The estimated values of ϵ at the transition are (see vertical lines in Fig. 14): $\epsilon_t \simeq 0.7k_B T$ ($\rho = 0.05$) and $\epsilon_t \simeq 0.65k_B T$ ($\rho = 0.1$). In comparison (see also Fig. 14), for the standard lattice-gas model, the transition values are roughly twice larger than these values: $\epsilon_t^{LG} \simeq 1.45k_B T$ ($\rho = 0.05$) and $\epsilon_t^{LG} \sim 1.3k_B T$ ($\rho = 0.1$).

Our computational results which show that the fluctuation mediated interactions reduce the strength of ϵ_t , are in a qualitative agreement with the mean field theory prediction. To make a quantitative comparison between the theory and the simulations, one needs to estimate the parameter B appearing in Eq.(35). Several reasons make such an estimation difficult and inaccurate: First, our non-standard mean field theory is based on the assumption that the clusters are circular and roughly have the same size, which is quite a crude approximation.

Second, tracing the precise location of ϵ_t in Fig. 14 is largely inaccurate because of the finite size of the system that makes the transitions look like crossovers. To reduce the large uncertainties associated with the determination of ϵ_t , one can look at the difference between the value of this quantity in our model of adhesion points and for the standard lattice-gas model. Using

$$\lambda_1^{\text{LG}} - \lambda_1 = 2\sqrt{\pi}B(\epsilon_t^{\text{LG}} - \epsilon_t), \quad (42)$$

for $\rho = 0.1$, we find $B \simeq 1$, as indeed expected for large clusters.

7 Conclusions

In this review we presented a statistical thermodynamics analysis of the aggregation behavior of adhesion points between a fluctuating membrane and a supporting surface. Our analysis focused on the contribution of the membrane thermal fluctuations to this process, via the attractive interactions that they mediate between the adhesion points. The origin of the fluctuation-induced (Casimir-like) interactions are the restrictions imposed on the membrane thermal fluctuations by the adhesion points, and the associated free energy cost which is minimized when the adhesion points localize in a cluster. We investigated both the two- and many-body fluctuation-induced interactions. For the two-body problem, our analysis reveals that the fluctuation induced pair potential is infinitely long-range with a logarithmic dependence on the pair distance. If, in addition to the excluded volume interactions, the membrane and the surface also interact via an attractive confining potential, the fluctuation-induced pair potential becomes screened at large distances. The screening of the pair potential is due to the fact that far away from each adhesion point, the amplitude of the fluctuations is governed by the strength of the external potential rather than by the presence of the other adhesion point.

In the many-body problem, the fluctuation-induced interactions are self-screened. The amplitude of the thermal fluctuations at each unit area of the membrane is governed by the distance to the closest adhesion points, which implies that each point interacts only with a few nearby points. This justifies our mapping of the problem into the 2D lattice-gas model with an effectively larger (“renormalized”) interaction energy. Depending on the strength of the renormalized

interactions, the system may be either in a “gas” (uniform distribution) or a “condensed” (adhesion cluster) phase. The interesting question which arises is whether the fluctuation-induced contribution to the attraction is sufficiently strong to allow cluster formation. Our analysis finds that the answer to this question is no. The fluctuation-induced interactions alone are too weak to induce the condensation transition. They do, however, greatly reduce (to below the thermal energy $k_B T$) the strength of the direct interactions at which the transition takes place.

Acknowledgment

I wish to express my deep gratitude to Prof. Phil Pincus for inspiring me to work on this fascinating problem. I have benefited enormously from many insightful discussions with him. I also wish to thank my student, Noam Weil, who participated in the final part of the research with such enthusiasm and creativity.

The work was supported by the Israel Science Foundation (Grant Number 946/08).

References

- [1] R. Lipowsky, E. Sackmann (Eds.), Handbook of Biological Physics: Structure and Dynamics of Membranes, Elsevier, Amsterdam, 1995.
- [2] B. Alberts, D. Bray, J. Lewis, M. Raff, K. Roberts, J. D. Watson, Molecular Biology of the Cell, Garland, New York, 1994.
- [3] T. Salditt, Thermal fluctuations and stability of solid-supported lipid membranes, J. Phys.: Condens. Matter 17 (2005) R287-R314.
- [4] M. Tanaka, E. Sackmann, Polymer-supported membranes as models of the cell surface, Nature 437 (2005) 656-663.
- [5] H. A. Rinia, G. W. H. Worpel, M. Müller, Visualization and characterization of domains in model membranes, in: A. Ottova-Tien (Ed.), Advances in Planar Lipid Bilayers and Liposomes Vol. 3, Elsevier, Amsterdam, 2006, pp.85-123.
- [6] M. Tanaka, E. Sackmann, Supported membranes as biofunctional interfaces and smart biosensor platforms, Phys. Stat. Sol. (a) 203 (2006) 3452-3462.
- [7] P. P. Girard, E. A. Cavalcanti-Adam, R. Kemkemer, J. P. Spatz, Cellular chemomechanics at interfaces: sensing, integration and response, Soft Matter 3 (2007) 307-326.
- [8] J. Salafsky, J. T. Groves, S. G. Boxer, Architecture and function of membrane proteins in planar supported bilayers: A study with photosynthetic reaction centers, Biochemistry 35 (1996) 14773-14781.
- [9] E. Sackmann, Supported membranes: Scientific and practical applications, Science 271 (1996) 43-48.
- [10] A. Kloboucek, A. Behirsch, J. Faix, E. Sackmann, Adhesion-induced receptor segregation and adhesion plaque formation: A model membrane study, Biophys. J. 77 (1999) 2311-2328.
- [11] Y. Kaizuka, T. J. Groves, Structure and dynamics of supported intermembrane junctions, Biophys. J. 86 (2004) 905-912.

- [12] A.-S. Smith, B. G. Lorz, U. Seifert, E. Sackmann, Antagonist-induced deadhesion of specifically adhered vesicles, *Biophys. J.* 90 (2006) 1064-1080.
- [13] A. Ananthakrishnan, A. Ehrlicher, The forces behind cell movement, *Int. J. Biol. Sci.* 3 (2007) 303-317.
- [14] P. S. Swain, D. Andelman, The influence of substrate structure on membrane adhesion, *Langmuir* 15 (1999), 8902-8914.
- [15] S. Komura, D. Andelman, The unbinding transition of mixed fluid membranes, *Europhys. Lett.* 64 (2003) 844-850.
- [16] K. R. Mecke, T. Charitat, F. Graner, Fluctuating lipid bilayer in an arbitrary potential: Theory and experimental determination of bending rigidity, *Langmuir* 19 (2003) 2080-2087.
- [17] M. I. Hoopes, M. Deserno, M. L. Longo, R. Faller, Coarse-grained modeling of interactions of lipid bilayers with supports, *J. Chem. Phys.* 129 (2008) 175102-1-175102-7.
- [18] M. C. Beckerle (Ed.), *Cell Adhesion*, Oxford University Press, Oxford, 2001.
- [19] D. A. Lauffenburger, J. Linderman, *Receptors: Models for binding, Trafficking, and Signaling*, Oxford University Press, Oxford, 1995.
- [20] A.-S. Smith, U. Seifert, Vesicles as a model for controlled (de-) adhesion of cells: a thermodynamic approach, *Soft Matter* 3 (2007), 275-289.
- [21] T. R. Weikl, M. Asfaw, H. Krobath, B. Różycki, R. Lipowsky, Adhesion of membranes via receptor-ligand complexes: Domain formation, binding cooperativity, and active processes, *Soft Matter* 5 (2009) 3213-3224.
- [22] P. F. Lenne, A. Nicolas, Physics puzzles on membrane domains posed by cell biology, *Soft Matter* 5 (2009), 2841-2848.
- [23] V. Niggli, Signaling to migration of neutrophils: importance of localized pathways, *Int. J. Biochem. Biochem Cell Biol.* 35 (2003) 1619-1638.

- [24] K. Giehl, A. Menke, Microenvironmental regulation of E-cadherin-mediated adherens junctions, *Front. Biosci.* 13 (2008) 3975-3985.
- [25] B. Geiger, A. Bershadsky, R. Pankov, K. M. Yamada, Transmembrane extracellular between the matrix-cytoskeleton crosstalk, *Nat. Rev. Mol. Cell Biol.* 2 (2001) 793-805.
- [26] A. G. Moreira, C. Jeppesen, F. Tanaka, C. M. Marques, Irreversible vs. reversible bridging: When is kinetics relevant for adhesion?, *Europhys. Lett.* 62 (2003) 876-882.
- [27] X. Zhang, V. T. Moy, Cooperative adhesion of ligand-receptor bonds, *Biophys. Chem.* 104 (2003) 271-278.
- [28] N. Gov, S. A. Safran, Pinning of fluid membranes by periodic harmonic potentials, *Phys. Rev. E* 69 (2004) 011101-1-011101-10.
- [29] T. Gruhn, R. Lipowsky, Temperature dependence of vesicle adhesion, *Phys. Rev. E* 71 (2005), 011903-1-011903-10.
- [30] G. Lomgo, I. Szleifer, Ligand-receptor interactions in tethered polymer layers, *Langmuir* 21 (2005), 11342-11351.
- [31] N. W. Moore, T. L. Kuhl, The role of flexible tethers in multiple ligand-receptor bond formation between curved surfaces, *Biophys. J.* 91 (2006) 1675-1687.
- [32] L. C.-L. Lin, J. T. Groves, F. L. H. Brown, Analysis of shape, fluctuations, and dynamics in intermembrane junctions, *Biophys. J.* 91 (2006) 3600-3606.
- [33] H. Krobath, G. J. Schütz, R. Lipowsky, T. R. Weikl, Lateral diffusion of receptor-ligand bonds in membrane adhesion zones: Effect of thermal membrane roughness, *Europhys. Lett.* 78 (2007) 38003-1-38003-6.
- [34] R.-J. Merath, U. Seifert, Fluctuation spectra of free and supported membrane pairs, *Eur. Phys. J. E* 23 (2007) 103-116.

- [35] M. Lamblet, B. Delord, L. Johannes, D. van Effenterre, P. Bassereau, Key role of receptor density in colloid/cell specific interaction: A quantitative biomimetic study on giant vesicles, *Eur. Phys. J. E* 26 (2008) 205-216.
- [36] E. Reister-Gottfried, K. Sengupta, B. Lorz, E. Sackmann, U. Seifert, A. Suncăna Smith, Dynamics of specific vesicle-substrate adhesion: From local events to global dynamics, *Phys. Rev. Lett.* 101 (2008) 208103-1-208103-4.
- [37] C. Selhuber-Unkel, M. Lopez-Garcia, H. Kessler, J. P. Spatz, Cooperativity in adhesion cluster formation during initial cell adhesion, *Biophys. J.* 95 (2008) 5424-5431.
- [38] J. Israelachvili, *Intermolecular and Surface Forces*, Academic Press, London, 1985.
- [39] B. Simon, *The Statistical Mechanics of Lattice Gases Vol. I*, Princeton University Press, Princeton, 1993.
- [40] J. Braun, J. R. Abney, J. C. Owicki, How gap junction maintains its structure, *Nature* 310 (1984) 316-318.
- [41] H. B. G. Casimir, On the attraction between two perfectly conducting plates, *Proc. K. Ned. Akad. Wet. B* 51 (1948), 793-796.
- [42] M. E. Fisher, P. G. de Gennes, Wall phenomena in a critical binary mixture, *C. R. Seances Acad. Sci. Ser. B* 287 (1978) 207-209.
- [43] M. Kardar, R. Golestanian, The “friction” of vacuum, and other fluctuation-induced forces, *Rev. Mod. Phys.* 71 (1999) 1233-1245.
- [44] M. Deserno, Mesoscopic membrane physics: Concepts, simulations, and selected applications, *Macromol. Rapid Commun.* 30 (2009) 752-771.
- [45] D. Frenkel, Introduction to colloidal systems, in: W. C. K. Poon, D. Andelman (Eds.), *Soft Condensed Matter Physics in Molecular and Cell Biology*, Taylor and Francis, New York, 2006, pp.19-47.
- [46] A. P. Gast, W. B. Russel, Simple ordering in complex fluids, *Phys. Today* 51 (1998) 24-30.

- [47] O. Farago, Membrane fluctuations near a plane rigid surface, *Phys. Rev. E* 78 (2008) 051919-1-051919-9.
- [48] W. Helfrich, Elastic properties of lipid bilayers: theory and possible experiments, *Z Naturforsch C*. 28 (1973) 693-703.
- [49] O. Farago, “Water-free” computer model for fluid bilayer membranes, *J. Chem. Phys.* 119 (2003) 596-605.
- [50] I. R. Cooke, K. Kremer, M. Deserno, Efficient tunable generic model for fluid bilayer membranes, *Phys. Rev. E* 72 (2005) 011506-1-011506-4.
- [51] G. Brannigan, L.C.-L. Lin, F. L. H. Brown, Implicit solvent simulation models for biomembranes, *Eur. Biophys. J.* 35 (2006) 104-124.
- [52] R. Bruinsma, M. Goulian, P. Pincus, Self-assembly of membrane junctions, *Biophys. J* 67 (1994) 746-750.
- [53] W . Helfrich, Steric interaction of fluid membranes in multilayer systems, *Z Naturforsch C*. 33A (1978) 305-315.
- [54] O. Farago, Fluctuation-induced attraction between adhesion sites of supported membranes, *Phys. Rev. E* 81 (2010) 050902(R)-1-050902(R)-4.
- [55] N. Weil and O. Farago, Entropy driven aggregation of adhesion sites of supported membranes, *Eur. Phys. J. E* 33 (2010) 81-87.